Draft version February 5, 2008
Preprint typeset using LaTeX style emulateapj v. 6/22/04

MODELING LUMINOSITY-DEPENDENT GALAXY CLUSTERING THROUGH COSMIC TIME

Charlie Conroy, Risa H. Wechsler[1], Andrey V. Kravtsov
Department of Astronomy and Astrophysics, Kavli Institute for Cosmological Physics, & The Enrico Fermi Institute, The University of Chicago, 5640 S. Ellis Ave., Chicago, IL 60637

Draft version February 5, 2008

ABSTRACT

We employ high-resolution dissipationless simulations of the concordance ΛCDM cosmology ($\Omega_0 = 1 - \Omega_\Lambda = 0.3$, $h = 0.7$, $\sigma_8 = 0.9$) to model the observed luminosity dependence and evolution of galaxy clustering through most of the age of the universe, from $z \sim 5$ to $z \sim 0$. We use a simple, non-parametric model which monotonically relates galaxy luminosities to the maximum circular velocity of dark matter halos ($V_{\rm max}$) by preserving the observed galaxy luminosity function in order to match the halos in simulations with observed galaxies. The novel feature of the model is the use of the maximum circular velocity at the time of accretion, $V_{\rm max}^{\rm acc}$, for subhalos, the halos located within virial regions of larger halos. We argue that for subhalos in dissipationless simulations, $V_{\rm max}^{\rm acc}$ reflects the luminosity and stellar mass of the associated galaxies better than the circular velocity at the epoch of observation, $V_{\rm max}^{\rm now}$. The simulations and our model $L-V_{\rm max}$ relation predict the shape, amplitude, and luminosity dependence of the two-point correlation function in excellent agreement with the observed galaxy clustering in the SDSS data at $z \sim 0$ and in the DEEP2 samples at $z \sim 1$ over the entire probed range of projected separations, $0.1 < r_p/(h^{-1}\ {\rm Mpc}) < 10.0$. In particular, the small-scale upturn of the correlation function from the power-law form in the SDSS and DEEP2 luminosity-selected samples is reproduced very well. At $z \sim 3-5$, our predictions also match the observed shape and amplitude of the angular two-point correlation function of Lyman-break galaxies (LBGs) on both large and small scales, including the small-scale upturn. This suggests that, like galaxies in lower redshift samples, the LBGs are fair tracers of the overall halo population and that their luminosity is tightly correlated with the circular velocity (and hence mass) of their dark matter halos.

Subject headings: cosmology: theory — dark matter — galaxies: halos — galaxies: evolution — galaxies:clustering — large-scale structure of the universe

1. INTRODUCTION

A generic prediction of high-resolution simulations of hierarchical Cold Dark Matter (CDM) models is that virialized regions of halos are not smooth, but contain subhalos — the bound, self-gravitating dark matter clumps orbiting in the potential of their host halo. The subhalos are the descendants of halos accreted by a given system throughout its evolution, which retain their identity in the face of disruption processes such as tidal heating and dynamical friction. Their presence is in itself a vivid manifestation of the hierarchical build-up of halo mass.

In the CDM scenario, luminous galaxies form via cooling and condensation of baryons in the centers of the potential wells of dark matter halos (White & Rees 1978; Fall & Efstathiou 1980; Blumenthal et al. 1984). In the context of galaxy formation, there is little conceptual difference between halos and subhalos, because the latter have also been genuine halos and sites of galaxy formation in the past, before their accretion onto a larger halo. We thus expect that each subhalo of sufficiently large mass should host a luminous galaxy and this is indeed supported by self-consistent cosmological simulations (e.g., Nagai & Kravtsov 2005). The observational counterparts of subhalos are then galaxies in clusters and groups or the satellites around individual galaxies. In this sense, we will use the term *halos* to refer to both distinct halos (i.e., halos not located within the virial radius of a larger system) and subhalos.

Although this general picture is definitely reasonable, it is not clear just how direct the relation between halos and galaxies is. One may argue, for example, that the subhalos can be disrupted much faster than the more tightly bound stellar system they host, leaving behind "orphan" galaxies (Gao et al. 2004; Diemand, Moore, & Stadel 2004). At the same time, properties of surviving subhalos, such as maximum circular velocity and gravitationally bound mass, are subject to strong dynamical evolution as they orbit within the potential of their host halo (e.g., Moore et al. 1996; Klypin et al. 1999; Hayashi et al. 2003; Kravtsov et al. 2004a; Kazantzidis et al. 2004). This makes the relation between subhalo properties and galaxy luminosity ambiguous (Nagai & Kravtsov 2005), because the latter may be less affected by dynamical processes but may evolve due to aging of the stellar populations after ram pressure strips the existing gas and the accretion of new gas is suppressed. The key question that we address in this paper is whether there is a one-to-one correspondence between populations of halos in dissipationless cosmological simulations and galaxies in the observable universe. As a test, we use comparisons of the predicted clustering of halos with the available observational measurements of galaxy clustering from $z \sim 5$ to the present.

During the last decade, large observational surveys of galaxies both at low and high redshifts have tremendously improved our knowledge of galaxy clustering, its evolution, and the relation between the galaxy and mat-

[1] Hubble Fellow

ter distributions. A coherent picture has emerged in which bright galaxies are strongly biased with respect to the matter distribution at high redshifts (Steidel et al. 1998; Giavalisco et al. 1998; Adelberger et al. 2003, 2005; Ouchi et al. 2004b, 2005; Lee et al. 2005; Hamana et al. 2005), and in which the bias decreases with time in such a way that the amplitude of galaxy clustering is only weakly evolving (e.g., Ouchi et al. 2004b), as expected in hierarchical structure formation (Colín et al. 1999; Kauffmann et al. 1999). The bias is also in general scale- and luminosity-dependent. Bright (red) galaxies are more strongly clustered than faint (blue) galaxies both in the local universe (Norberg et al. 2002; Zehavi et al. 2004, 2005, and references therein) and in the distant past (Coil et al. 2004, 2005b).

A recent development is the detection of a departure from a pure power law in the two-point correlation function of galaxies at $z \sim 0$ (Zehavi et al. 2004, 2005). This departure is expected in general because the two-point correlation function is a sum of two separate contributions: the one-halo term, which arises from pairs of galaxies within a distinct dark matter halo, and the two-halo term, which arises from pairs of galaxies from two different distinct halos (e.g., Cooray & Sheth 2002). The one-halo contribution dominates on small scales, while at scales larger than the size of the largest virialized regions clustering is due to the two-halo term. The two terms are not generically expected to combine so as to give a power-law correlation function. The deviation of the correlation function from a power-law was *predicted* to be even stronger at higher redshifts (Zheng 2004; Kravtsov et al. 2004b), and this has now been convincingly confirmed (Adelberger et al. 2005; Ouchi et al. 2005; Lee et al. 2005; Hamana et al. 2005) using galaxy samples identified with the Lyman-break technique (Steidel et al. 1996, 1999).

Despite impressive advances in the amount and quality of data on the galaxy distribution over a wide range of redshifts, the exact relation between dark matter halos and luminosity- or Lyman-break-selected galaxies is still rather uncertain (e.g., Mo et al. 1999; Kolatt et al. 1999; Wechsler et al. 2001). The most popular attempts to connect the dark halos and luminous galaxies employ semi-analytic modeling (e.g., White & Frenk 1991; Kauffmann et al. 1994; Avila-Reese et al. 1998; Somerville & Primack 1999; Cole et al. 1994, 2000; Croton et al. 2005; Bower et al. 2005), which uses phenomenological recipes for specifying when, where, and how galaxies form within dark matter halos, often in conjunction with high-resolution dissipationless simulations. Another popular approach is to use the halo model (see e.g. Cooray & Sheth 2002, and references therein), which, in its simplest form, specifies the probability distribution for a particular halo of mass M to host a given number of galaxies N with specified properties, such as luminosity, color, etc. More complex halo models include the conditional luminosity function (CLF) approach (Yang et al. 2003; Cooray 2005a,b) which specifies the luminosity function for halos of mass M, and models which connect other features (e.g., Vale & Ostriker 2004; Neyrinck, Hamilton, & Gnedin 2005).

While these approaches manage to capture the general observational trends, they usually employ a large number of free parameters, making it difficult to glean the relevant underlying mechanism(s) responsible for the agreement between the model and data. Most implementations also do not provide a direct constraint on the relation between luminous components of galaxies and dark matter halos. In fact, *assumptions* are made about this relation in most cases.

In this study we use galaxy clustering to address two straightforward issues. First, we question whether current data is consistent with a one-to-one correspondence between luminous galaxies and galaxy-sized dark matter halos in cosmological simulations. Second, we ask whether the observed clustering is consistent with a simple relation between galaxy luminosity and some property of its host halo. In the context of the second question, we investigate which halo properties are most closely related to galaxy luminosity. We show with the currently available data the answer to both of these questions is yes, as we can reproduce luminosity-dependent clustering measurements at different redshifts from $z \sim 5$ to $z \sim 0$ with a simple, non-parametric model relating galaxy luminosity to the halo circular velocity.

Although a number of studies during the last decade have shown that galaxy clustering can be approximately matched by the clustering of dark matter halos in dissipationless simulations (Carlberg 1991; Brainerd & Villumsen 1992, 1994b,a; Colín, Carlberg, & Couchman 1997; Wechsler et al. 1998; Colín et al. 1999; Kravtsov & Klypin 1999; Kravtsov et al. 2004b; Neyrinck et al. 2004) the size of observational samples did not allow thorough tests of the galaxy-halo relation. For example, Kravtsov et al. (2004b) and Neyrinck et al. (2004) compare the two-point correlation function of halos and bright galaxies from the SDSS and PSCz surveys, respectively, and find good agreement on scales $0.1 \lesssim r/(h^{-1}\ \mathrm{Mpc}) \lesssim 10$. However, these studies do not attempt to match the clustering of fainter galaxies. Tasitsiomi et al. (2004) assign luminosities to halos and compute the galaxy-mass correlation function, finding good agreement for two broad luminosity bins, after a reasonable amount of scatter was introduced into the relation.

The current work extends these analyses by comparing results of very high-resolution simulations to the most current measurements of the two-point correlation functions over a wide range of luminosities and redshifts. The large size and wide luminosity range of observational samples allows us to test the relation between galaxy luminosities and properties of their host halos with unprecedented power. The novel feature of the simulation analysis we present is that for each halo and subhalo we track the evolution of its properties, such as mass and maximum circular velocities. As we show below, this is a key piece of information for reasons that are easy to understand. For distinct halos, the current circular velocity is a measure of their potential well built-up during evolution, and can therefore be expected to be tightly correlated with the stellar mass (or more generally the baryonic mass) of the galaxy the halo hosts. The circular velocity of subhalos in dissipationless simulations, on the other hand, is a product of both mass buildup during the period when the halo evolved in isolation *and* tidal mass loss after the halo starts to orbit within the virialized region of a larger object and experience strong tidal forces (Hayashi et al. 2003; Kravtsov et al.

2004a; Kazantzidis et al. 2004). The stellar component of the galaxies, which should be more tightly bound than halo dark matter, should not be significantly affected by tidal forces and can stabilize the mass distribution (and hence $V_{\rm max}$) in the inner regions. We can therefore expect that luminosity and stellar mass of galaxies hosted by halos in dissipationless simulations should be correlated with the subhalo mass or circular velocity, $V_{\rm max}^{\rm acc}$, *at the epoch of accretion*, rather than with its current value. This is borne out by cosmological simulations, which include gas dynamics, cooling, and star formation (Nagai & Kravtsov 2005) who show that selection using $V_{\rm max}^{\rm acc}$ results in subhalo properties similar to the selection based on stellar mass of galaxies subhalos host. One can therefore argue that a reasonable approach is to relate galaxy luminosity to the current halo circular velocity for distinct halos and to the circular velocity at accretion for subhalos. The main result of this study is that this simple model reproduces the luminosity-dependence of galaxy clustering at different epochs with remarkable, and perhaps surprising, accuracy. We note that Vale & Ostriker (2005) have recently presented and used a semi-analytic model for subhalos, which employs a similar approach to luminosity assignment, except that they use the total bound halo mass instead of circular velocity.

The paper is organized as follows. In §2 we briefly describe the simulations, halo finding algorithm, and the method for tracking the evolution of halos. §3 details our method for relating halos to galaxies, and elaborates upon our motivation for using $V_{\rm max}^{\rm acc}$ as the basis for the luminosity assignment for subhalos. In §4 we compare observational clustering results over the redshift interval $0 < z < 5$ to the clustering of halos in dissipationless ΛCDM simulations. The halo occupation distribution implied by this model is described in §5. In §6 we discuss the implications of our results and in §7 we summarize our main conclusions. Throughout this paper we assume a ΛCDM cosmology with $(\Omega_m, \Omega_\Lambda, h, \sigma_8) = (0.3, 0.7, 0.7, 0.9)$.

2. THE SIMULATIONS

The simulations used here were run using the Adaptive Refinement Tree (ART) N-body code (Kravtsov et al. 1997; Kravtsov 1999). The ART code implements successive refinements in both the spatial grid and temporal step in high density environments. These simulations were run in the concordance flat ΛCDM cosmology with $\Omega_m = 0.3 = 1 - \Omega_\Lambda$, $h = 0.7$, where Ω_m and Ω_Λ are the present-day matter and vacuum densities in units of the critical density, and h is the Hubble parameter in units of 100 km s^{-1} Mpc^{-1}. The power spectra used to generate the initial conditions for the simulations were determined from a direct Boltzmann code calculation (courtesy of Wayne Hu). We use a power spectrum normalization of $\sigma_8 = 0.90$, where σ_8 is the rms fluctuation in spheres of $8h^{-1}$ Mpc comoving radius.

To study the clustering properties of dark matter halos over a range of scales, we consider two simulations of the above cosmology The first simulation, L80, followed the evolution of 512^3 particles in a $80h^{-1}$ Mpc box. The L80 simulation has a particle mass of $m_p = 3.16\times10^8\ h^{-1}M_\odot$ and peak force resolution $h_{\rm peak} = 1.2\ h^{-1}$ kpc. This is the simulation to which we make most comparisons with observations. The second simulation we consider is denoted L120 and was run with 512^3 particles in a 120 h^{-1} Mpc box, resulting in a particle mass of $m_p = 1.07\times10^9\ h^{-1}M_\odot$ and peak force resolution $h_{\rm peak} = 1.8\ h^{-1}$ kpc. This simulation thus has a larger particle mass and somewhat lower spatial resolution compared to the L80 run. We use this simulation to obtain better statistics for the correlation function of rare (i.e., massive) objects.

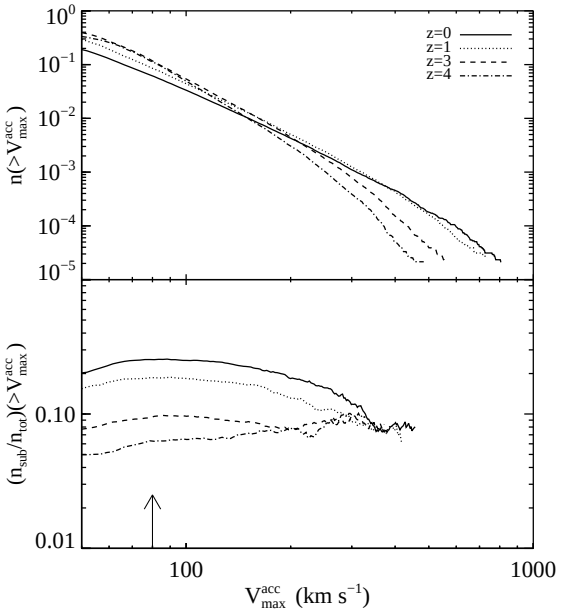

FIG. 1.— *Top panel*: Cumulative velocity function for all halos identified in the L80 simulation at various redshifts, in units of h^3 Mpc^{-3}. *Bottom panel*: Fraction of subhalos as a function of redshift and maximum circular velocity at the time of accretion, $V_{\rm max}^{\rm acc}$. We truncate the curves where $N_{\rm sub} < 10$ because in that regime poisson noise washes away any useful information. The arrow delimits our nominal completeness limit.

2.1. *Halo Identification, Classification, and Construction of Merger Trees*

Our analysis requires detailed dynamical knowledge of not only distinct halos, i.e. halos with centers that do not lie within any larger virialized system, but also subhalos which are located within the virial radii of larger systems. Note that the term "halo" (e.g., the *halo* occupation distribution) usually refers to what we call distinct halos in this work.

We identify distinct halos and the subhalos within them using a variant of the Bound Density Maxima (BDM) halo finding algorithm (Klypin et al. 1999). Details of the algorithm and parameters used can be found in Kravtsov et al. (2004b); we briefly summarize the main steps here. All particles are assigned a density using the `smooth` algorithm[2] which uses a symmetric SPH smoothing kernel on the 32 nearest neighbors. Starting with the highest overdensity particle, we surround each potential center by a sphere of radius $r_{\rm find} = 50h^{-1}$ kpc and exclude all particles within this sphere from further search. Hence no two halos can be separated by less than

[2] To calculate the density we use the publicly available code `smooth: http://www-hpcc.astro.washington.edu/tools/tools.html`

$r_{\rm find}$. We then construct density, circular velocity, and velocity dispersion profiles around each center, iteratively removing unbound particles as described in Klypin et al. (1999). Once unbound particles have been removed, we measure quantities such as $V_{\rm max} = \sqrt{GM(<r)/r}|_{\rm max}$, the maximum circular velocity of the halo. For each distinct halo we calculate the virial radius, defined as the radius enclosing overdensity of 180 with respect to the *mean* density of the Universe at the epoch of the output. We use this virial radius to classify objects into distinct halos and subhalos. The halo catalog is complete for halos with more than 50 particles which corresponds, for the L80 simulations, to a minimum halo mass of $1.6 \times 10^{10} h^{-1}\ M_\odot$.

For subhalos we also tabulate $V_{\rm max}^{\rm acc}$, the maximum circular velocity at the time when a subhalo falls into a distinct halo. In order to tabulate this quantity we rely on merger trees generated for these simulations, which track the histories of both distinct halos and subhalos. A detailed description of the merger tree construction is given in Allgood (2005). The merger trees we use here follow halo evolution through 48 timesteps between $z = 7$ and the present for the L80 box and 89 timesteps for the L120 box. For each subhalo, we use the merger trees to step back in time until the subhalo is no longer identified as belonging to a larger system. We then define $V_{\rm max}^{\rm acc}$ to be $V_{\rm max}$ of the subhalo at that time.

In the top panel of Figure 1 we show the cumulative velocity function for all identified halos from $z = 4$ to 0. This figure quantifies the relation between $V_{\rm max}^{\rm acc}$ and n, as we will use these two quantities interchangeably to define our halo samples throughout the paper. In the bottom panel we show the corresponding cumulative fraction of subhalos as a function of time. The figure shows that the subhalo fraction is a weak function of circular velocity at all epochs. There is a weak trend for a smaller subhalo fraction among halos with larger $V_{\rm max}^{\rm acc}$. There is a stronger trend of increasing subhalo fraction with decreasing redshift.

3. CONNECTING GALAXIES TO HALOS

In this section we motivate and describe our model for associating galaxies with dark matter halos. We make this connection by relating galaxy luminosity and a physical property of dark matter halos, for which we choose $V_{\rm max}^{\rm now}$ for distinct halos and $V_{\rm max}^{\rm acc}$ for subhalos. As discussed above, for subhalos $V_{\rm max}^{\rm acc}$ denotes the maximum circular velocity *at the time the subhalo was accreted*. The maximum of the circular velocity profile, $V_{\rm max}$, is a measure of the depth of the halo potential well and is expected to correlate strongly with stellar mass of the galaxies, as implied by the Tully-Fisher and Faber-Jackson relations. At the same time, the definition of $V_{\rm max}$ in simulations is unambiguous both for distinct halos and subhalos, which is not the case for the total mass, as different operational definitions are used by different authors. It should be noted that $V_{\rm max}$ used here will not correspond directly to $V_{\rm max}$ observed in, for example, the Tully-Fisher relation because dissipationless simulations do not take into account the effect of baryon condensation on $V_{\rm max}$ (e.g., Blumenthal et al. 1986).

The use of $V_{\rm max}^{\rm acc}$ for subhalos is the novel feature

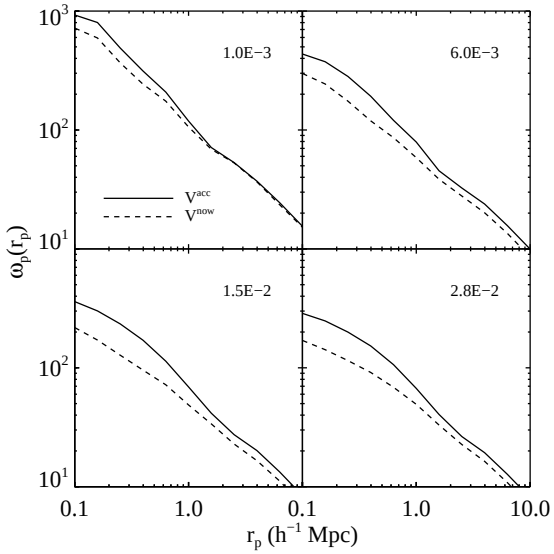

FIG. 2.— Projected two-point correlation function at $z \sim 0$ comparing the effects of selecting on $V_{\rm max}^{\rm acc}$ (solid lines) versus $V_{\rm max}^{\rm now}$ (dashed lines) at four different number density thresholds (labeled in the top right corner, in units of h^3 Mpc^{-3}). While there is a slight increase in the correlation function on large scales when using $V_{\rm max}^{\rm acc}$ rather than $V_{\rm max}^{\rm now}$, the difference is much stronger on small scales. The difference between $V_{\rm max}^{\rm acc}$ and $V_{\rm max}^{\rm now}$ is due to the tidal stripping of subhalos which have fallen into larger systems, hence correlation functions will be most strongly effected on small scales.

of our model[3]. As we discussed in the introduction, the motivation for this is fairly straightforward. While $V_{\rm max}$ decreases due to tidal stripping as a halo falls through a larger halo (Hayashi et al. 2003; Kravtsov et al. 2004a), one can expect that the stellar component of galaxies within these halos will not be affected appreciably since stars are concentrated near the bottom of the halo potential well and are more tightly bound (e.g., Nagai & Kravtsov 2005). Hence we argue that, for galaxies associated with subhalos, luminosity should correlate more strongly with $V_{\rm max}^{\rm acc}$ than the $V_{\rm max}^{\rm now}$ affected by dynamical evolution. Therefore, throughout the rest of the paper, unless explicitly stated otherwise, the maximum circular velocity, $V_{\rm max}$, will be assumed to mean:

$$V_{\rm max} = \begin{cases} V_{\rm max}^{\rm acc}, & \text{subhalos} \\ V_{\rm max}^{\rm now}, & \text{distinct halos} \end{cases} \quad (1)$$

Although it is not clear how accurate this assumption is in detail, we show that it provides a considerably better match to observed galaxy clustering compared to the uniform selection using $V_{\rm max}^{\rm now}$ for both subhalos and distinct halos. Note also that the use of circular velocities before accretion can also help explain the abundance of faint dwarf galaxies in the Local Group (Kravtsov et al. 2004a).

In order to assign luminosities, we assume a monotonic relation between galaxy luminosity and $V_{\rm max}$ and

[3] As we prepared this paper for publication, Vale & Ostriker (2005) submitted a paper in which they employ a semi-analytic model for subhalos and a similar approach to luminosity assignment, except that they use the total bound halo mass instead of circular velocity.

require that the $L-V_{\rm max}$ relation preserves the galaxy luminosity function (LF). Specifically, we use the following equation:

$$n_g(> L_i) = n_h(> V_{{\rm max},i}) \quad (2)$$

where n_g and n_h are the number density of galaxies and halos, respectively. We stress again, that $V_{\rm max}$ in the above expression is equal to $V_{\rm max}^{\rm acc}$ for subhalos and to $V_{\rm max}^{\rm now}$ for distinct halos (for which the accretion epoch is undefined). For each L_i we find the corresponding $V_{\rm max,i}$ such that the above relation is satisfied. The main assumption is therefore that there is a monotonic relation between galaxy luminosity and $V_{\rm max}$. The model makes no further assumptions and is completely non-parametric. This should be kept in mind when we compare *predictions* of this model to observed galaxy clustering. Note that we do not take any possible scatter in the $L-V_{\rm max}$ relation into account in this model.

With the $L-V_{\rm max}$ relation in hand, comparing observational clustering statistics to the model predictions is straightforward: we simply compute the desired statistic for the halos with assigned luminosities corresponding to the observed sample luminosity range. This method does not currently treat other galaxy properties such as color, although it could conceivably be extended to include such properties. We have not included the possibility of "orphaned galaxies", i.e. galaxies without any associated subhalos. We discuss the issue of orphans in detail in §6.

Figure 2 shows the effect that selection of halos using $V_{\rm max}^{\rm acc}$ rather than $V_{\rm max}^{\rm now}$ for subhalos has on the projected two-point correlation function $\omega_{\rm p}$ for different number densities, at $z = 0$. As expected, the effect is most significant on small scales, where the subhalo contribution dominates, and the difference between $V_{\rm max}^{\rm acc}$ and $V_{\rm max}^{\rm now}$ is greatest.

In Figure 3 we show the effect of selecting halos according to $V_{\rm max}^{\rm acc}$ and $V_{\rm max}^{\rm now}$ on the galaxy-mass cross-correlation function, ξ_{gm}. The small bump in the sample selected using $V_{\rm max}^{\rm acc}$ in the top panel is due to the fact that $V_{\rm max}^{\rm acc}$ samples in general have more satellites than $V_{\rm max}^{\rm now}$ samples, and the satellite contribution to ξ_{gm} peaks near $r_{\rm p} = 0.5\ h^{-1}$ Mpc. The "bump" is smaller in the lower panel, where the $V_{\rm max}$ threshold is much higher, because the number of satellites is nearly the same between the $V_{\rm max}^{\rm acc}$ and $V_{\rm max}^{\rm now}$ selected samples in this case.

At higher redshifts the differences between samples selected using $V_{\rm max}^{\rm acc}$ and $V_{\rm max}^{\rm now}$ are small.[4] Figure 4 shows the projected correlation function for the $V_{\rm max}^{\rm acc}$- and $V_{\rm max}^{\rm now}$-selected samples at four redshifts. The samples are constructed to have a fixed number density $n = 1.5 \times 10^{-2} h^3$ Mpc^3. The situation is similar for other number densities. Already by $z \sim 1$ the effect of selection is quite small. The difference on small scales for the $z \sim 3$ and $z \sim 4$ samples is not statistically significant.[5]

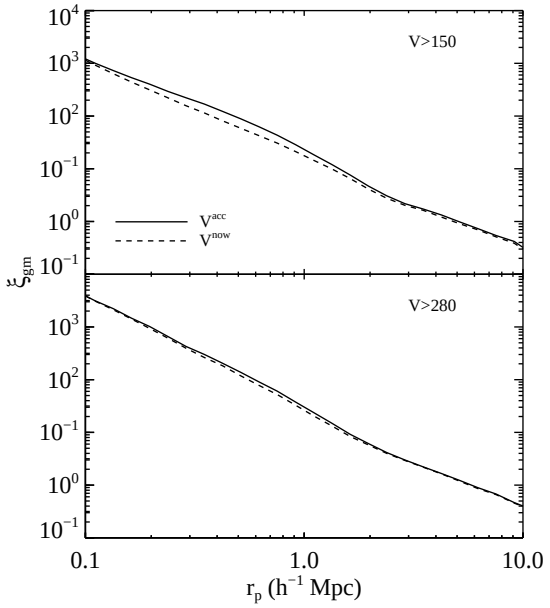

FIG. 3.— Comparison of the galaxy-mass cross-correlation function for halos selected using $V_{\rm max}^{\rm acc}$ (solid lines) and $V_{\rm max}^{\rm now}$ (dashed lines) at two different circular velocity thresholds (labeled in the top right corner of each panel, in units of km s^{-1}).

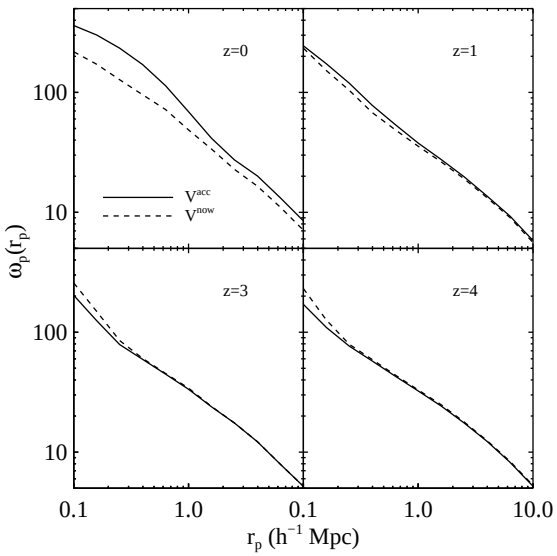

FIG. 4.— Comparison of the projected two-point correlation function for halos selected using $V_{\rm max}^{\rm acc}$ (solid lines) and $V_{\rm max}^{\rm now}$ (dashed lines) at four different redshifts, for a fixed number density, $n = 1.5 \times 10^{-2} h^3$ Mpc^{-3}. This figure clearly shows that, while using $V_{\rm max}^{\rm acc}$ over $V_{\rm max}^{\rm now}$ results in a large difference at low redshift, it has very little impact at higher redshifts. The trend is similar for a wide range of number densities.

[4] Note that the designation "now" refers to the time of observation, not to $z = 0$.

[5] Note that at high z the correlation function at the smallest scales is somewhat higher for the $V_{\rm max}^{\rm now}$-selected samples, which seems counter-intuitive. We believe that this is a small artefact of the halo finding algorithm. At higher redshifts, the halos are smaller and subhalos are typically at smaller distances from the host center. At small radii the removal of unbound particles is more difficult as the halos are located near the bottom of the potential well. The value of $V_{\rm max}^{\rm now}$ in such cases can be overestimated producing a boost in the number of subhalos above a given threshold value, and boosting the correlation function somewhat. Note, however, that the effect is small and the difference between correlation functions for $V_{\rm max}^{\rm now}$- and $V_{\rm max}^{\rm acc}$-selected samples is less than 2σ.

We believe that this effect can be attributed to the distribution of accretion times for subhalos at each redshift: at low redshift, subhalos have a wide distribution of accretion times, and hence a large number of subhalos have had time to experience significant tidal stripping, while at higher redshifts the distribution of accretion times rises sharply near the epoch of observations. This is because both the accretion and disruption rates are high at high redshifts. The accreted halos do not survive for a prolonged period of time, so that at each high-z epoch most of identified subhalos are recently accreted objects, which are yet to experience significant tidal mass loss.

Since we are only computing $V_{\rm max}^{\rm acc}$ for subhalos which have survived to the current epoch, one may worry that we are neglecting a significant population of subhalos with a sizeable $V_{\rm max}^{\rm acc}$ that are not present in the halo catalog at the current epoch. Of such a population there can only be two fates: either the object was at some point physically disrupted or it has simply fallen below the resolution limit. We have used the merger trees to find all subhalos which have ever fallen into a distinct halo and have tabulated their $V_{\rm max}^{\rm acc}$ and the ratio in mass between the subhalo and distinct halo, at the time of accretion. For a wide range in $V_{\rm max}^{\rm acc}$ thresholds, the distribution of mass ratios is strongly peaked between 0.1 and 1.0. This implies that dynamical friction has caused the subhalo to merge with the distinct halo on the order of a dynamical time, and suggests that the majority of these subhalos have in fact physically merged and should not have survived. The absence of such missing subhalos also implies that in our simulations there should be no "orphan" galaxies (Gao et al. 2004, see § 6 for further discussion of this issue).

4. GALAXY CLUSTERING FROM $Z \sim 5$ TO THE PRESENT

In this section we compare clustering statistics of halos to recent observations of the galaxy two-point correlation function over the redshift interval $0 \lesssim z \lesssim 5$. The observed clustering statistics we compare to are $\omega_p(r_p)$, the projected two-point correlation function, and $\omega(\theta)$, the angular two-point correlation function. We estimate ω_p by integrating the real space, three-dimensional correlation function, $\xi(r)$, computed in the simulation, along the line of sight:

$$\omega_p(r_p) = 2\int_0^\infty \xi(\sqrt{r_p^2 + r_\parallel^2})dr_\parallel, \qquad (3)$$

where the comoving distance r has been decomposed into perpendicular (r_p) and parallel to the line-of-sight ($r_\parallel$) components. In practice, the integration in Eqn. 3 is truncated at some finite scale: we truncate at $40h^{-1}$ Mpc for SDSS galaxies (§4.1) and $20h^{-1}$ Mpc for DEEP2 galaxies (§4.2), as is done in the data. Since the simulation box size is only $80h^{-1}$ Mpc, the measurement of $\xi(r)$ is not reliable for $r \gtrsim 0.1L_{\rm box} \sim 8h^{-1}$ Mpc. To extrapolate $\xi(r)$ to larger scales, we use $\xi_m(r)$, the two-point correlation function of dark matter [6], multiplied by the linear bias of $\xi(r)$ measured over $4 < r/(h^{-1}{\rm Mpc}) < 8$.

[6] We derive the dark matter correlation function from the power spectrum provided by the publicly available code of Smith et al. (2003), which is more accurate than the popular Peacock and Dodds prescription.

Generating $\omega(\theta)$ from $\xi(r)$ without assuming $\xi(r)$ to be a power law is somewhat more involved. With knowledge of the redshift distribution, $N(z)$, of the sample, $\omega(\theta)$ can be derived via the Limber transformation:

$$\omega(\theta) = \frac{\int_0^\infty dz N^2(z) \int_{-\infty}^\infty dx \xi(\sqrt{[D_m(z)\theta]^2 + x^2})/R_H(z)}{[\int_0^\infty dz N(z)]^2} \qquad (4)$$

where $D_m(z)$ is the proper motion distance and $R_H(z)$ is the Hubble radius at redshift z. As for $\omega_{\rm p}$, the integral over $\xi(r)$ is in practice truncated at a finite scale; we integrate to 50 h^{-1} Mpc and note that the resulting $\omega(\theta)$ is not sensitive to this particular truncation scale.

4.1. *Clustering at $z \sim 0$*

The SDSS (York et al. 2000; Abazajian et al. 2004) is a large photometric and spectroscopic survey of the local Universe. Zehavi et al. (2005) have measured the luminosity and color dependence of $w_p(r_p)$ for $\sim 200,000$ SDSS galaxies over ≈ 2500 deg^2 with $z < 0.15$. As mentioned in §3, assigning $V_{\rm max}$ to galaxy luminosity while preserving the observed luminosity function (LF) results in a unique $L{-}V_{\rm max}$ relation. In order to make the assignment we use the SDSS luminosity function presented in Blanton et al. (2003), with Schechter (1976) parameters in the r-band $M_r^* - 5{\rm log}h = -20.5$, $\alpha = -1.05$, and $\phi^* = 1.5 \times 10^{-2}h^{-3}$ Mpc^3. It is then straightforward to compare the observed luminosity dependence of both the small and large scale clustering of SDSS galaxies to our model.

The results for luminosity threshold samples ($L > L_{\rm th}$) are shown in the left panel of Figure 5, where we compare the Zehavi et al. (2005) results to the clustering of halos corresponding to the range of galaxy luminosities in each sample. For the three halo samples with $n = 6 \times 10^{-3}h^3$ Mpc^{-3}, $n = 1.5 \times 10^{-2}h^3$ Mpc^{-3} and $n = 2.8 \times 10^{-2}h^3$ Mpc^{-3} we use the L80 simulation, while for the halo sample with $n = 1.1 \times 10^{-3}h^3$ Mpc^{-3} we use the L120 simulation in order to improve statistics. See Table 1 for details of the SDSS samples used here. The agreement is excellent over all scales. We find similar agreement when $w_p(r_p)$ is measured in differential, rather than integral, luminosity bins. It is critical to realize that the agreement on scales $r_p \lesssim 1h^{-1}$ Mpc is due to our luminosity assignment scheme using $V_{\rm max}^{\rm acc}$. The luminosity assigned using $V_{\rm max}^{\rm now}$ for subhalos would result in a significant under-prediction of amplitude of $\omega_{\rm p}$ at $r_{\rm p} \lesssim 1h^{-1}$ Mpc, especially for fainter samples (see Figure 2).

The halo occupation distribution (HOD) specifies the distribution of the number of galaxies within a (distinct) halo of mass M, $P(N|M)$. It has become a popular tool for interpreting galaxy clustering (Jing et al. 1998; Seljak 2000; Scoccimarro et al. 2001; Bullock, Wechsler, & Somerville 2002; Yan, Madgwick, & White 2003; Berlind et al. 2003; Zehavi et al. 2005; Kravtsov et al. 2004b; Zheng 2004; Abazajian et al. 2005; Tinker et al. 2005), which requires that the first two moments of $P(N|M)$ be specified to calculate two-point clustering. In the right panel of Figure 5 we show the first moment of this distribution, the average number of galaxies within a (distinct) halo of mass M, $\langle N(M)\rangle$, for the four halo samples which correspond to the four luminosity threshold SDSS samples in the left panels. As expected,

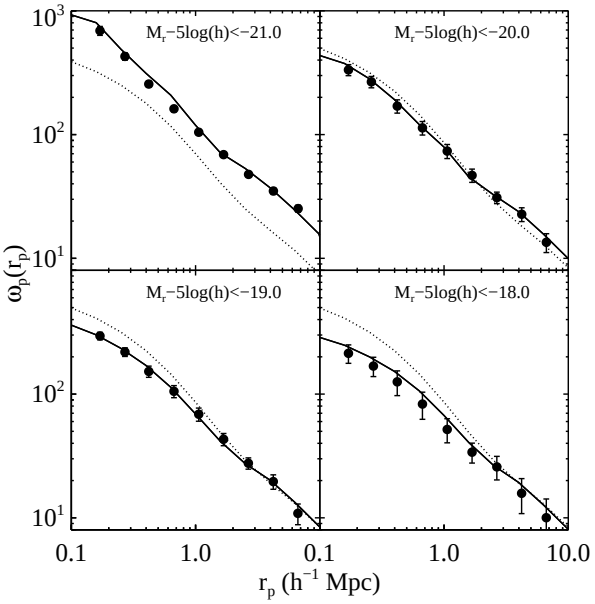

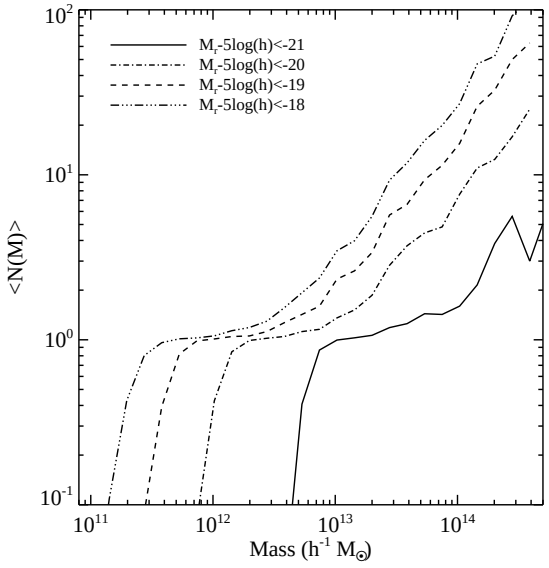

FIG. 5.— *Left:* Comparison between the SDSS projected correlation function (points) and the correlation function derived from halos (solid lines) for various luminosity threshold samples. For comparison we include the correlation function of dark matter particles (dotted lines) at the median redshift of the sample. *Right:* The first moment of the halo occupation distribution (HOD) for the four halo samples. For all four samples, the gradual roll-off at small mass is due to scatter in the $V_{\rm max}$ -mass relation. The fan (dotted lines) corresponds to slopes of 0.4, 0.7, and 1.0.

the halo samples corresponding to brighter galaxy samples reside preferentially in more massive distinct halos. The halo sample corresponding to the brightest galaxies ($M_r - 5\log h < -21$) rarely has more than one halo per distinct halo. All three halo samples display a gradual roll-off in $\langle N(M)\rangle$ at low mass which is simply due to scatter in the $V_{\rm max}$ -mass relation, as we select samples using $V_{\rm max}$, but plot as a function of mass. See §5 for a more detailed discussion of the HOD associated with this model.

The good agreement between the observed galaxy correlation function and samples of halos with our L−$V_{\rm max}$ model, over a range of luminosities and scales, suggests that the luminosity dependence of galaxy clustering is due primarily to how galaxies form within dark matter halos. This implies that galaxy properties vary as a function of larger scale environment only insofar as the halos in which the galaxies reside vary.

4.2. *Clustering at $z \sim 1$*

The DEEP2 Galaxy Redshift Survey (Davis et al. 2004) has gathered optical spectra for $\sim 50,000$ galaxies at $z \sim 1$ using the DEIMOS spectrograph on the Keck II 10-m telescope. The survey, recently completed, spans a comoving volume of $\sim 10^6 h^{-3}$ Mpc^3, covering 3 deg^2 over four widely separated fields. We use the DEEP2 B-band luminosity function of Willmer et al. (2005) to compute the L−$V_{\rm max}$ relation at $z \sim 1$. A Schechter fit to the overall luminosity function yields $M_B^* - 5\log h = -20.73$ and $\phi^* = 8.7\times10^{-3}h^{-3}$ Mpc^3 with α fixed at $\alpha = -1.30$. A detailed comparison has shown that these values are consistent with other estimates of the global luminosity function at $z \sim 1$ (Faber et al. 2005).

The projected two-point correlation function, $\omega_p(r_p)$, has been measured for DEEP2 galaxies as a function of luminosity and color (Coil et al. 2004, 2005b,a). In addition, Coil et al. (2005b) has estimated the two-point cross correlation between galaxies and groups, and be-

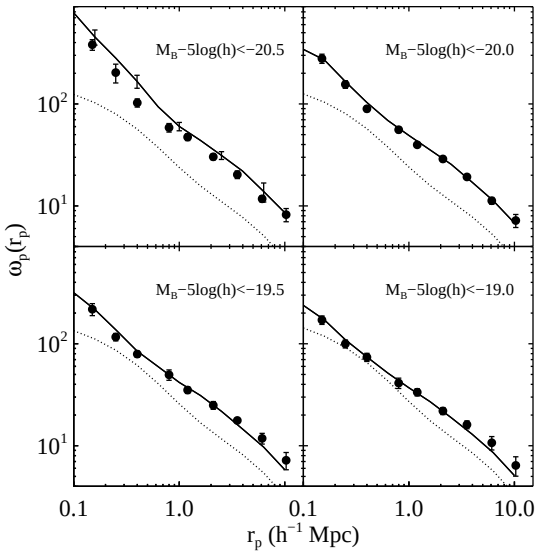

FIG. 6.— Projected two-point correlation function at $z \sim 1$ for DEEP2 galaxies (solid circles) and halos (solid lines), at four different luminosity thresholds. We include jack-knife errors, computed using the eight octants of the simulation cube, on the model prediction for the brightest sample to demonstrate that they agree within 1σ. The excellent agreement on all scales for these four samples suggests that luminosity-dependent clustering is a result of two effects: a simple relation between galaxy luminosities and dark matter halos, and the spatial clustering of the halos. For comparison, we include the correlation function of dark matter particles (dotted lines).

tween group centers and group galaxies, based on the group catalog of Gerke et al. (2005). For the following comparisons we use the most recent measurements of $\omega_p(r_p)$ derived from the completed survey (Coil et al. 2005a).

Figure 6 compares the projected two-point correlation function for DEEP2 galaxies in four luminosity threshold samples to the clustering of corresponding dark matter halos. For the $M_B - 5\log h < -19.0$, -19.5, and -20.0 samples we use the L80 simulation, while for the $M_B - 5\log h < -20.5$ sample we use the L120 simulation to improve statistics. Slight discrepancies on small scales for the $M_B - 5\log h < -20.5$ sample may be attributed to cosmic variance and poisson noise in a sample of this number density, and in fact our smaller L80 box provides a slighly better match to the data. Overall the agreement is excellent on all scales for all four samples[7].

We would like to stress again that this remarkable agreement is achieved using the halo distribution in *dissipationless* simulations using a simple, non-parametric relation between galaxy luminosity and halo circular velocity. The luminosity-dependent bias at $z \sim 1$ hence seems to be driven entirely by the fact that brighter galaxies reside in more massive halos, with the correspondence between halo and luminosity determined by matching the observed luminosity function to the dark matter halo velocity function.

4.3. *Clustering at $z > 2$*

Very little was known about the clustering properties of galaxies at $z \geq 2$ until the advent of the Lyman-break technique (Steidel & Hamilton 1993; Steidel et al. 1996, 1999, 2003). This technique allows the identification of high-redshift Lyman-break galaxies (LBGs) by optical photometry alone, using information about the well-defined region in color-color space that these objects occupy. While simple color-color cuts allow one to gather large numbers of LBG candidates with relative ease, it should be kept in mind that this technique is not perfect. Accurate completeness numbers are difficult to estimate, but it is believed that the Lyman-break technique successfully identifies $80-90\%$ of real LBGs (specific completeness numbers depend on limiting apparent magnitude, dataset — e.g., ground observations or the HST, and sample definition, among other unknowns, and is often estimated via Monte Carlo simulations of artificial LBGs; see Adelberger et al. 2004; Ouchi et al. 2004a; Lee et al. 2005).

The level of contamination, or the fraction of false positives, is more important when considering the clustering of LBGs because such objects can artificially dilute or enhance the observed signal. At $z \sim 3$ the main source of contamination is Galactic stars (4%) and high-redshift active galactic nuclei (3%), as determined by extensive spectroscopic follow-up (Steidel et al. 2003). At higher redshifts the situation is less certain, as there has to date been much less spectroscopic follow-up. Ouchi et al. (2005) estimate the contamination for their $z \sim 4$ sample based on Subaru data at $\sim 5\%$ from spectroscopic follow-up of 63 LBG candidates. LBG candidates extracted from the GOODS survey avoid Galactic star contamination thanks to high angular resolution of the HST (Lee et al. 2005), although other sources of contamination remain unquantified.

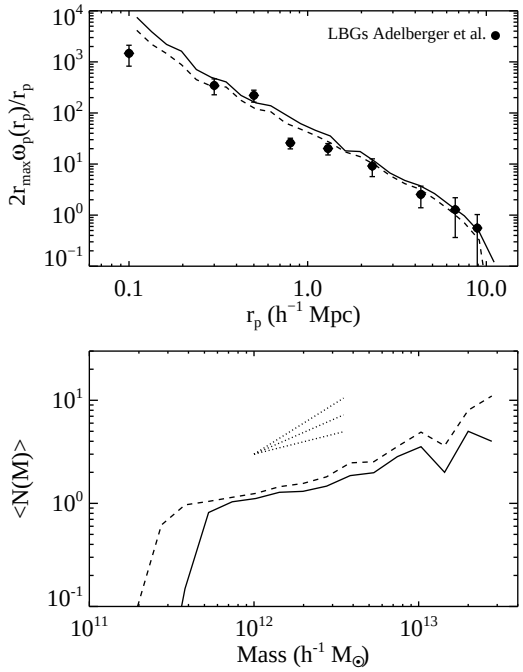

FIG. 7.— Comparison between $z \sim 3$ LBGs and dark matter halos in simulations. *Top panel*: the projected correlation function measured from 700 spectroscopically confirmed LBGs (solid circles, Adelberger et al. 2003), compared to halos at the same number density, $n = 4 \times 10^{-3} h^3$ Mpc^{-3} (solid line) and halos twice as numerous, $n = 8 \times 10^{-3} h^3$ Mpc^{-3} (dashed line). *Bottom panel*: The number of halos per distinct halo for the two halo samples. The fan (dotted lines) corresponds to slopes of 0.4, 0.7, and 1.0.

In this section all quoted number densities have been completeness and contamination corrected. If the completeness is well estimated, then using the corrected number density should mitigate any incompleteness effects. However, even if the number density is contamination corrected, in order to fairly compare the clustering of LBGs to dark matter halos we must include the clustering properties of these contaminants. For simplicity, when estimating the effects of contamination we will assume the contaminants to have a random distribution on the sky. (We need not include additional clustering effects in the completeness case because in this case the missing objects are LBGs, which are assumed to have the same clustering properties as the identified LBGs, but note that this assumption would break down if the LBG completeness was a strong function of luminosity.)

Since the early result (Steidel et al. 1998) that Lyman-Break Galaxies are a strongly clustered population, there have been numerous attempts to use their clustering properties to connect these galaxies to their host dark matter halos (e.g., Wechsler et al. 1998; Jing & Suto 1998; Adelberger et al. 1998; Katz et al. 1999; Mo et al. 1999; Wechsler et al. 2001; Giavalisco & Dickinson 2001; Bullock et al. 2002; Scannapieco & Thacker 2003). There have been two popular explanations for the properties of these galaxies: some have speculated that they are a quiescent star-

[7] Booyah!

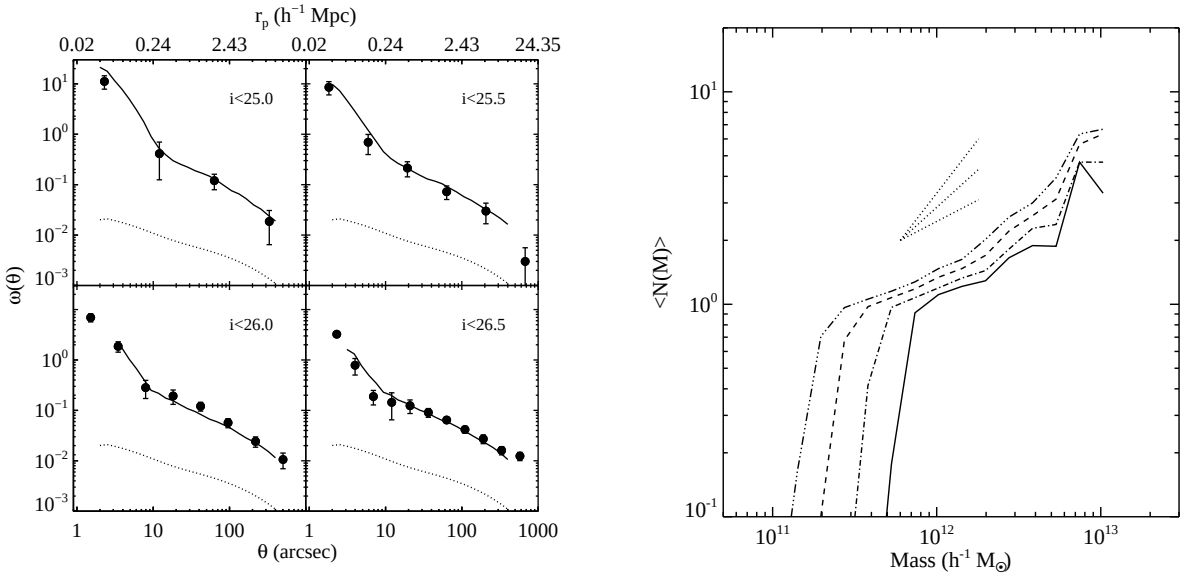

FIG. 8.— *Left:* Two-point correlation function of $z \sim 4$ LBGs derived from Subaru data (solid circles, Ouchi et al. 2005) compared to the correlation function for halos at the same number density (solid lines). The four panels correspond to four different apparent magnitude limits, and hence different number densities (see Table 1 for a summary of the Subaru data). The dotted line is $\omega(\theta)$ for dark matter particles at $z \sim 4$. *Right:* Average number of member galaxies for halos corresponding to the four Subaru samples at $z \sim 4$. The lines correspond to the Subaru samples, from left to right, $i < 26.5$, $i < 26.0$, $i < 25.5$, and $i < 25.0$. The fan (dotted lines) corresponds to slopes of 0.4, 0.7, and 1.0.

forming population of the most massive galaxies (e.g. Coles et al. 1998; Mo et al. 1999; Giavalisco & Dickinson 2001), while others have suggested that they are more related to temporal events such as merger-driven starbursts (Lowenthal et al. 1997; Kolatt et al. 1999; Somerville et al. 2001; Scannapieco & Thacker 2003). The extent to which either of these scenarios can be ruled out by the clustering data has been a matter of some debate, depending on the detailed assumptions that were made in each case (see Wechsler et al. 2001 for a review of these issues).

Our results for LBGs at $z \sim 3$ are shown in Figure 7. In the top panel we plot the two-point projected correlation function for 700 spectroscopically confirmed LBGs (Adelberger et al. 2003) with an estimated number density of $n = 4 \times 10^{-3} h^3$ Mpc^{-3} at $\bar{z} = 2.9$. Note that this sample does not suffer contamination problems because these LBGs are spectroscopically confirmed. We plot ω_p for halos in units identical to those in Adelberger et al. (2003, where $r_{\rm max}$ is the line-of-sight distance through which we count projected pairs). We measure $\omega_p(r_p)$ for halos at two different number densities to illustrate that a factor of two uncertainty in the LBG number density (a larger uncertainty than is quoted in Adelberger et al. 2003) does not alter these results. The figure shows that the agreement between the clustering of halos and LBGs is quite good.

In the bottom panel of Figure 7 we show the halo occupation of galaxies for the halo samples we associate with $z \sim 3$ LBGs. As expected, the halo sample which has a higher number density (dashed lines), and a correspondingly lower $V_{\rm max}$ threshold, has a lower cutoff in $\langle N(M) \rangle$. The measured halo occupation implies that most distinct halos are host to a single LBG. $\langle N(M) \rangle$ rises above 2 only for the most massive halos ($\gtrsim 10^{13} h^{-1} M_\odot$), which are very rare at $z \sim 3$.

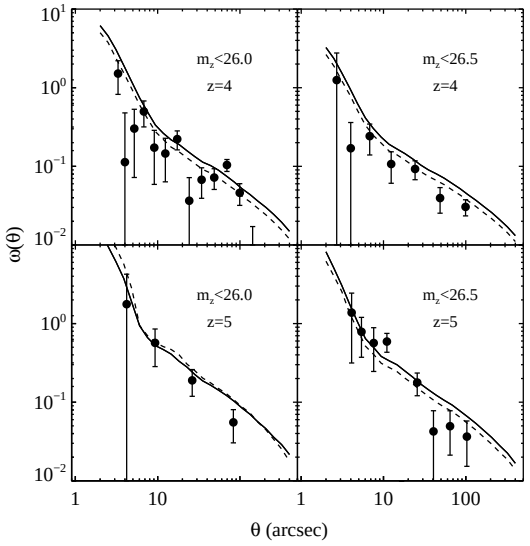

FIG. 9.— Two-point correlation function of LBGs measured using GOODS data (solid circles, Lee et al. 2005), compared to the correlation function of halos at the same number density (solid lines). We also show the effect of a 10% contamination in the identification of LBGs (dashed lines). *Top panels*: B-band dropouts which correspond to $z \sim 4$, at apparent magnitude limits of $m_z < 26.0$ (left) and $m_z < 26.5$ (right). *Bottom panels*: V-band dropouts corresponding to $z \sim 5$ at apparent magnitude limits, $m_z < 26.0$ (left), and $m_z < 26.5$ (right). See Table 1 for a summary of the GOODS data used here.

At still higher redshifts the clustering of LBGs has recently been measured in two separate datasets: by

Ouchi et al. (2005) using Subaru data and by Lee et al. (2005) using the HST GOODS survey. These authors detect a strong departure from a power law in the angular two-point correlation function of LBGs. When parameterized in the framework of the halo model, this excess small scale ($\theta < 10''$) power is attributed to multiple galaxies within a distinct halo, i.e. the '1-halo' term. We now compare our $L-V_{\rm max}$ model to these data.

The left panel of Figure 8 compares the angular correlation function of LBGs from Ouchi et al. (2005) to the angular correlation function of halos for four different apparent magnitude thresholds, at $z \sim 4$. If the identified LBGs occupy a relatively narrow range of redshifts, as expected, then these apparent magnitude cuts should correspond to absolute magnitude limits. The agreement is again remarkably good on all the scales we probe. Our non-parametric $L-V_{\rm max}$ model captures the luminosity dependence of LBG clustering, on both large and small scales, correctly predicts the scale of the small-scale upturn in $\omega(\theta)$, and the fact that this scale decreases for increasing number density. The latter trend is due to a decrease in the typical mass (and size) of the distinct halos hosting LBGs as the number density is increased. We do not plot the correlation function for halos below $r_p \approx 50h^{-1}$ kpc since the halo finder we use does not find halos closer than this separation.

Connecting with previous work, we show in the right panel of Figure 8 the halo occupation, $\langle N(M)\rangle$, for the halo samples which correspond to the $z \sim 4$ Subaru samples. Increasingly brighter LBG samples reside in preferentially larger mass distinct halos. Furthermore, since $\langle N(M)\rangle < 2$ for $M < 10^{13}h^{-1}M_\odot$, our $L-V_{\rm max}$ model implies that the majority of these highest-redshift LBGs live alone in distinct dark matter halos. This picture is in qualitative agreement with previous analysis of the LBG clustering in the framework of halo model (Lee et al. 2005; Ouchi et al. 2005).

Figure 9 compares the clustering of LBGs from GOODS data at $z \sim 4$ (top panels) and $z \sim 5$ (bottom panels) to the clustering of halos at similar redshifts and number densities. Here again the agreement is very good, even at $z \sim 5$. The model somewhat overpredicts the clustering of the fainter sample at $z = 4$. In this plot we also show the effect of a contaminated LBG sample, i.e. we assume that 10% of identified LBGs are actually interlopers with a random distribution on the sky. The effect of contamination scales $\omega(\theta)$ by $(1-c)^2$, where c is the contamination fraction. A 10% contamination reduces the angular correlation function by $\approx 20\%$ and results in better agreement for the fainter GOODS samples (right panels) which plausibly have higher contamination than the brighter samples. We note that 10% contamination is likely an upper limit and was included here for illustration purposes. The detailed spectroscopic follow-up of these high redshift samples have yet to yield direct accurate estimates of contamination fractions.

The straightforward implication of the presented comparisons is that the data is consistent with, and one could argue supports, the picture in which most LBGs are the central galaxies in their host halos with luminosity tightly related to the halo circular velocity and mass. Most LBGs have no neighbors within the same halo. However, a fraction of them do and it is this fraction that is responsible for the strong upturn in the correlation function at small scales. By accurately reproducing both the small-scale upturn in $\omega(\theta)$ and the large-scale clustering, our model accurately predicts not only the correct distinct halos to associate with LBGs (the '2 halo term' in halo model jargon) but also the number of LBGs within a distinct halo (the corresponding '1 halo term').

TABLE 1
Summary of Samples

Data	Defn.[a]	$\bar{z}$ [b]	$n/10^{-3}$ h^3 Mpc^{-3}	$V_{\rm max}$ [c] km s^{-1}
SDSS	$M_r < -18$	0.04	27.0	110
SDSS	$M_r < -19$	0.06	15.0	130
SDSS	$M_r < -20$	0.06	6.0	180
SDSS	$M_r < -21$	0.15	1.1	310
DEEP2	$M_B < -19.0$	0.87	13.0	150
DEEP2	$M_B < -19.5$	0.92	8.4	170
DEEP2	$M_B < -20.0$	0.98	4.9	200
DEEP2	$M_B < -20.5$	0.99	2.5	250
Adelberger	U_nGR colors	2.9	4.0	207
Subaru	$i < 25.0$	4	0.8	265
Subaru	$i < 25.5$	4	1.9	225
Subaru	$i < 26.0$	4	3.8	191
Subaru	$i < 26.5$	4	6.4	174
GOODS	$m_z < 26.0$, B-drop	4	2.7	205
GOODS	$m_z < 26.5$, B-drop	4	4.5	185
GOODS	$m_z < 26.0$, V-drop	5	1.5	200
GOODS	$m_z < 26.5$, V-drop	5	2.6	180

[a] Absolute SDSS and DEEP2 magnitudes are in units of $M - 5\log(h)$.
[b] Mean redshift of sample; for Subaru and GOODS data, $\bar{z}$ is based on Monte Carlo simulations of artificial LBGs.
[c] $V_{\rm max}$ such that $n(> V_{\rm max}) = n_{\rm sample}$ for halos at the simulation output closest to $\bar{z}$.

5. DEPENDENCE OF HALO OCCUPATION ON NUMBER DENSITY AND REDSHIFT

In this section we explore the redshift and number density dependence of the halo occupation distribution (HOD), the key ingredient of the halo model, in our $V_{\rm max}-L$ assignment scheme. We compare our results to previous studies which fit the halo occupation to observational clustering data. The HOD, or the probability distribution for a distinct halo of mass M to host N galaxies, provides a relatively clean and simple framework for interpreting clustering data. The two-point correlation function in the halo model depends on the first and second moments of the HOD ($\langle N\rangle$ and $\langle N(N-1)\rangle$, respectively).

The first moment of the HOD can be separated into two components (e.g., Kravtsov et al. 2004b):

$$\langle N(M)\rangle = \langle N(M)\rangle_{\rm cen} + \langle N(M)\rangle_{\rm sat}, \qquad (5)$$

where $\langle N(M)\rangle_{\rm cen}$ and $\langle N(M)\rangle_{\rm sat}$ are the number of central and satellite galaxies (i.e., subhalos), respectively. The central galaxy term is a step function rising to $\langle N(M)\rangle_{\rm cen} = 1$ above a minimum distinct halo mass, $M_{\rm min}$. Kravtsov et al. (2004b) show that distribution of the subhalo occupation at fixed M is well-modeled by a Poisson distribution; this continues to hold well in the simulations presented here. Although some authors model the cutoff at $M_{\rm min}$ to take into account scatter between the observable and host halo mass, we model this

term as a step-function for simplicity, and note that this simplification will only impact the $M_{\rm min}$ parameter.

The satellite term, $\langle N(M)\rangle_{\rm sat}$, can be described by a power-law function, $\langle N(M)\rangle_{\rm sat} \propto M^{\alpha}$, for large distinct halo masses. Kravtsov et al. (2004b) and Zheng et al. (2005) find that $\alpha \approx 1$ for subhalos and galaxies identified in cosmological simulations within massive distinct halos, over a wide range of number density thresholds (corresponding to luminosity threshold) cuts. For small distinct halo masses, $\langle N(M)\rangle_{\rm sat}$ "rolls-off" faster than the power law. Kravtsov et al. (2004b) describe the "roll-off" by:

$$\langle N(M)\rangle_{\rm sat} = (M/M_1 - C)^{\alpha}. \quad (6)$$

Tinker et al. (2005) propose an alternative exponential form for the "roll-off":

$$\langle N(M)\rangle_{\rm sat} = \frac{M}{M_1}\exp\left(-\frac{M_{\rm cut}}{M}\right), \quad (7)$$

where $M_{\rm cut}$ and M_1 are free parameters, this time with the asymptotic slope fixed at $\alpha = 1$. In fact, we find that $M_{\rm cut}$ and M_1 are tightly correlated such that

$$\log(M_{\rm cut}) = 0.76\log(M_1) + 2.3, \quad (8)$$

for the full range of number densities and redshifts explored here, thereby reducing Equation 7 to a one-parameter function. As shown in Figure 11, this form is an excellent fit to the number of satellite halos in our simulations over a large range of redshifts and number densities. We have explicitly checked the asymptotic slopes of $\langle N(M)\rangle_{\rm sat}$ where possible and find that they are consistent with $\alpha = 1$, in agreement with previous theoretical predictions (Kravtsov et al. 2004b).

The exponential functional form of Equation 7 is preferable to Equation 6 because for a given choice of parameters M_1 and C, $\langle N(M)\rangle_{\rm sat}$ can become negative using the latter. For example, best-fit values for these parameters for the $z \sim 0$, $n = 20.0 \times 10^{-3}$ h^3 Mpc^{-3} sample (triangles in the top left panel of Figure 11) implies that $\langle N(M)\rangle_{\rm sat}$ will be negative for $M \sim 2 \times 10^{12}$ $h^{-1}M_{\odot}$, which is not in agreement with the results of simulations. For this reason we choose to use Equation 7 to describe the functional form of $\langle N(M)\rangle_{\rm sat}$.

Note that the presence of the "roll-off" is important, and neglecting it can bias the best-fit HOD parameters. Zehavi et al. (2005) use

$$\langle N(M)\rangle_{\rm sat} = (M/M_1)^{\alpha} \quad (9)$$

to model the clustering of SDSS galaxies at $z \sim 0$ and find that α increases for galaxies of increasing luminosity. However, in the presence of the roll-off at small M, brighter samples will have on average fewer satellites and hence $\langle N(M)\rangle_{\rm sat}$ will be dominated by the steeper exponential cut-off. A power-law fit is hence expected to yield artificially steep slopes. Indeed, when fitting a pure power law without this roll-off to $\langle N(M)\rangle_{\rm sat}$ in the simulations, we find slopes closer to $\alpha \approx 1.5$.

In Table 2 we list the best-fit HOD parameters for halos in our simulations over a wide range of number densities and redshifts. The corresponding halo occupations are plotted in Figure 10, while Figure 11 shows the contribution from subhalos (satellites) alone.

With the HOD in hand we can derive several useful quantities. The average number of halos per distinct halo,

$$\langle N\rangle = \frac{\int_{M_{\rm min}}^{\infty}\langle N(M)\rangle n_{\rm halo}(M)dM}{\int_{M_{\rm min}}^{\infty} n_{\rm halo}(M)dM} \quad (10)$$

and the average mass of distinct halos (member number weighted),

$$\langle M\rangle = \frac{\int_{M_{\rm min}}^{\infty}\langle N(M)\rangle n_{\rm halo}(M)MdM}{\int_{M_{\rm min}}^{\infty} n_{\rm halo}(M)dM} \quad (11)$$

are useful when considering a 'typical' halo in a given

TABLE 2
HOD parameters and derived quantities

n/10^{-3} h^3 Mpc^{-3}	z	log($M_{\rm min}$)	log(M_1)	log($M_{\rm cut}$)	$\langle N\rangle$	log($\langle M\rangle$)
1.0	0	12.8	14.0	13.1	1.15	13.6
1.0	1	12.7	13.7	12.7	1.16	13.2
1.0	3	12.1	12.0	12.0	1.15	12.5
1.0	4	11.8	12.4	12.1	1.16	12.2
4.0	0	12.3	13.5	12.4	1.22	13.4
4.0	1	12.1	13.3	12.4	1.14	12.9
4.0	3	11.7	12.8	12.1	1.08	12.2
4.0	4	11.5	12.5	11.8	1.08	11.8
8.0	0	12.0	13.1	12.4	1.27	13.4
8.0	1	11.9	13.0	12.3	1.17	12.8
8.0	3	11.5	12.6	11.9	1.08	12.0
8.0	4	11.2	12.3	11.6	1.08	11.7
20.0	0	11.5	12.7	12.0	1.32	13.4
20.0	1	11.5	12.7	11.9	1.20	12.7
20.0	3	11.1	12.4	11.6	1.09	11.8
20.0	4	10.9	12.1	11.5	1.07	11.5

Note. — All quoted masses are in units of $h^{-1}M_{\odot}$.

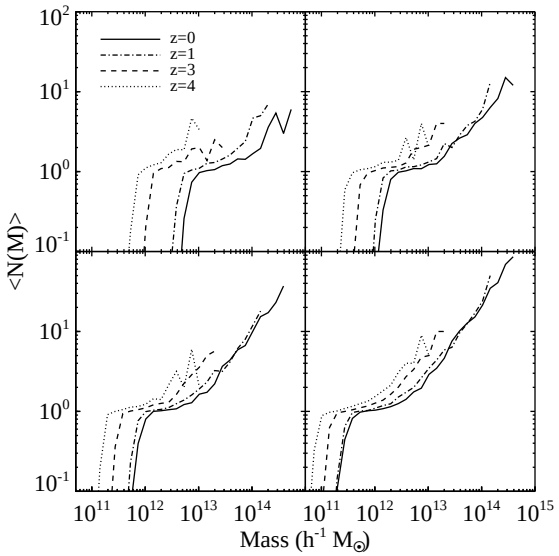

Fig. 10.— Evolution of the halo occupation, $\langle N(M)\rangle$ from $z \sim 4$ to 0 at fixed number density (clockwise from top left: $n = 1.0$, 4.0, 20.0, and 8.0, in units of $10^{-3}h^3$ Mpc^{-3}).

sample. These two quantities are included in Table 2. Note that when computing these quantities we use the halo occupation measured directly from simulations (shown in Figure 10) rather than the best-fit halo occupation implied by equations 5 and 7.

The redshift evolution of $\langle N(M)\rangle$ for samples of fixed number density reveals several interesting trends. The minimum mass of the sample, or the location of the step in the mean occupation number, is decreasing with increasing redshift, reflecting evolution of the halo mass function. At higher redshifts, the halos hosting multiple satellites become more rare, so that in most samples the high-M power-law tail of $\langle N(M)\rangle_{\rm sat}$ is not present. This trend is apparent in Figure 11 which shows the redshift evolution of $\langle N(M)\rangle_{\rm sat}$ for halo samples of different number densities. At the same time, the "shoulder" (or the region between the step and the power-law tail) in $\langle N(M)\rangle$ becomes shorter and not as flat at higher z (Fig. 10), reflecting the increasing fraction of relatively small-mass halos hosting more than a single central galaxy. We choose to characterize the extent of the shoulder via the ratio $M_1/M_{\rm min}$. As can be seen by consulting Table 2, this ratio (and hence the shoulder) decreases both with decreasing number density and increasing redshift. As we will discuss more thoroughly below, we believe that it is the extent of the shoulder which is primarily responsible for the upturn in the correlation function on small scales. Hence samples with a lower number density and/or at higher redshift (and hence a smaller shoulder) should have a more significant upturn in $\omega_p(r_p)$ on small scales, as is observed.

The HOD parameters we derive are in good qualitative agreement with observations. At $z\sim 0$, Zehavi et al. (2005) fit a different functional form for $\langle N(M)\rangle_{\rm sat}$ (namely Eqn. 9), and hence a direct comparison is complicated. However, $M_{\rm min}$ is unaffected by the functional form for $\langle N(M)\rangle_{\rm sat}$, and here the values quoted in Table 2 are in excellent agreement with Zehavi et al. (2005). The trend of M_1 to decrease with increasing number density is also in agreement with the derived results from observations.

A direct comparison to the HOD derived in the literature for LBGs is again complicated. The parameters given in Table 2 are *predicted* by our simulations, while most analyses *assume* a pure power-law form for the overall halo occupation and fit for the parameters in the framework of the halo model (Hamana et al. 2005; Lee et al. 2005; Ouchi et al. 2005). The assumed power-law form does not describe HOD in our simulations well. This is an example illustrating that HOD fitting is in general not unique — different functional forms can simultaneously match the number density and 2-point clustering of a sample. Because derived quantities such as $\langle N\rangle$ and $\langle M\rangle$ are entirely dependent on the form of the HOD, it is critical to realize that these derived quantities are also not unique. Despite the different forms for $\langle N(M)\rangle$, we find here similar qualitative trends for the average distinct halo mass of LBGs, namely that fainter samples (corresponding to higher number densities) have smaller $\langle M\rangle$, as is seen in Ouchi et al. (2005) and Lee et al. (2005). As emphasized by Bullock, Wechsler, & Somerville (2002), this degeneracy may be partially broken by looking at the smallest scale clustering information available (typically parameterized as the close-pair counts); a comparison with the most recent data of this sort from $z\sim 0-1$ is being pursued for a similar model to ours by Berrier et al (in preparation).

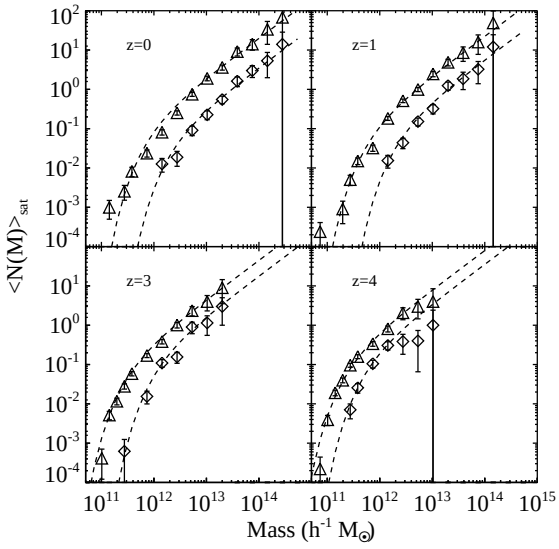

FIG. 11.— $\langle N(M)\rangle_{\rm sat}$ as a function of number density and redshift. Diamonds designate halo samples at $n = 4.0\times10^{-3}\ h^3$ Mpc^{-3}, triangles are for samples with $n = 20.0\times10^{-3}\ h^3$ Mpc^{-3}. The dashed lines corresponds to Eqn. 7, with the best-fit parameters listed in Table 2.

As was shown in §3, selecting subhalos according to $V_{\rm max}^{\rm acc}$ results in an enhanced clustering signal compared to using $V_{\rm max}^{\rm now}$, especially on small scales and at low redshifts, because there are more subhalos in the $V_{\rm max}^{\rm acc}$ selected sample. To illustrate this directly, we fit Eqn. 7 to satellites selecting in these two different ways. We find that the effect of using $V_{\rm max}^{\rm acc}$ over $V_{\rm max}^{\rm now}$, insofar as there are more satellites at fixed distinct halo mass, is small for low masses, and gradually increases toward higher masses. In other words, the difference in $\langle N(M)\rangle$ is small near the exponential cutoff while $V_{\rm max}^{\rm acc}$-selected samples show steeper $\langle N(M)\rangle$ with increasing M for higher masses.

To understand this trend consider the following. In order for there to exist a sizable difference between $V_{\rm max}^{\rm acc}$ and $V_{\rm max}^{\rm now}$, a subhalo must orbit within a distinct halo for a sufficient amount of time such that tidal stripping can reduce $V_{\rm max}$. Dynamical friction, which depends on the relative masses of subhalos to distinct halos, will be much stronger in lower distinct halo masses because there exists a minimum halo mass corresponding to our $V_{\rm max}$ threshold. In other words, as one considers smaller distinct halo masses for a given $V_{\rm max}$ threshold, the typical subhalo mass cannot be arbitrarily close to the host mass because such halos would suffer efficient dynamical friction and would merge quickly without significant evolution of $V_{\rm max}$. At higher distinct halo masses, dynamical friction is not efficient for the typical subhalo since now the typical subhalo is much less massive than the distinct halo, and hence a subhalo can exist within a distinct halo for a sufficient amount of time for tidal stripping to have a significant effect on $V_{\rm max}$.

6. DISCUSSION

Following the reliable identification of subhalos in N-body simulations, there has been a concerted effort to identify such subhalos with observed galaxies. A persistent problem with this approach is that subhalos selected using the present-day mass or circular velocity tend to have radial distributions within their larger distinct halos that are shallower than those exhibited by observed galaxies (Gao et al. 2004; Diemand et al. 2004; Nagai & Kravtsov 2005; Macció et al. 2005). However, Nagai & Kravtsov (2005) find that the observed radial profile of galaxies can be reproduced by selecting subhalos using stellar mass, rather than the present day total mass. We argue that the best proxy for the stellar mass in dissipationless simulations is the current maximum circular velocity for distinct halos and the circular velocity at the time of accretion, $V_{\rm max}^{\rm acc}$, for subhalos.

We have shown that this simple, non-parametric model which relates galaxy luminosities to the maximum circular velocity of dark matter halos, $V_{\rm max}$, by preserving the observed galaxy luminosity function, accurately reproduces the observed luminosity-dependent clustering of galaxies over projected separations $0.1 < r_p/(h^{-1}$ Mpc$) < 10.0$, from $z \sim 5$ to $z \sim 0$. The only assumption of the model is that there is a monotonic relation between galaxy luminosity and halo circular velocity. To assign luminosities we use the maximum circular velocity at the time of accretion, $V_{\rm max}^{\rm acc}$, for subhalos, and the maximum circular velocity at the time of observation, $V_{\rm max}^{\rm now}$, for distinct halos. This ingredient is crucial for accurately reproducing the observed clustering of galaxies at $z \sim 0$.

The success of the model has several important implications. First, our results indicate that dissipationless simulations do not suffer from significant overmerging because they reproduce both the amplitude and shape of the correlation function and the underlying HOD quite accurately. If our dissipationless simulations were missing a significant fraction ($\gtrsim 40\%$) of objects in groups and clusters, as suggested by some recent studies (Gao et al. 2004; Diemand et al. 2004), both the amplitude and shape of the correlation function in these simulations would be grossly incorrect. We also note that recent analysis of the observed galaxy-mass cross correlation function disfavors the existence of a large population of satellites without associated dark matter halos (Mandelbaum et al. 2005).

In order to assess the quantitative impact of a fraction of "orphan" galaxies — satellite galaxies with no identifiable subhalo (Gao et al. 2004) — in our model, we perform the following test. We artificially increase the fraction of subhalos in such a way that the subhalo occupation function, $\langle N(M)\rangle_{sat}$ increases in amplitude while maintaining the same shape. In order to match the observed galaxy luminosity function, we simulatenously increase the overall $V_{\rm max}$ threshold for a given sample, such that the number density does not change. We find that an orphan fraction $> 10\%$ is inconsistent with the correlation functions of the SDSS galaxy samples at $z \sim 0$ for all luminosities (for this cosmological model and the assumption of no scatter between L and $V_{\rm max}^{\rm acc}$).

Our results also imply that the central assumption of the luminosity assignment model — the tight, monotonic relation between galaxy luminosity and halo circular velocity — likely exists for the observed galaxies. Such a relation is indeed expected (e.g., Mo et al. 1998) for isolated galaxies, but our results indicate that this is true globally for galaxies of different types and for a wide range of redshifts. We argue that for subhalos the dissipation should result in a centrally condensed, tightly-bound stellar system which would stabilize the halo circular velocity against tidal heating. Stellar mass and luminosity of galaxies should therefore correlate with the circular velocity of subhalos at the time they are accreted, before significant tidal evolution takes place. Given that we match luminosity at a particular epoch to the circular velocity at different epochs (the epoch of observation for distinct halos, and the epoch of accretion for subhalos), a subtle implication of our scheme is that the relation between luminosity and $V_{\rm max}$ does not evolve strongly with time — a result which may have been anticipated by the lack of scatter in the Tully–Fisher relationship in different environments.

The corollary is then that the clustering of a particular galaxy sample is largely determined by the clustering of halos and subhalos that host the galaxies. Clustering of halos and subhalos is governed by gravitational dynamics (e.g., Kravtsov & Klypin 1999; Zentner et al. 2005, and discussion therein), while the particular subset of halos that host galaxies in a given sample is determined by the relations between observable galaxy properties and properties of their host dark matter halos *and* selection criteria used to define the sample. In the case of the galaxy luminosity, the relation with halo circular velocity appears to be particularly tight.

The model agreement with the clustering properties of the LBG population at $3 < z < 5$ is perhaps more surprising, given that the LBG selection criteria are significantly more complicated than those of the luminosity-selected samples at $z \leq 1$. The success of our L–$V_{\rm max}$ model indicates that the rest-frame LBG luminosity is likely to be tightly related to the halo circular velocity (and hence total mass). This would, in turn, suggest that LBGs are fair tracers of the overall halo population rather than a special subset of halos, such as halos undergoing mergers or collisions. Although we have not explicitly investigated the latter scenarios (i.e., mergers or collisions), it seems unlikely that the observed LBG clustering would be well matched by a model in which the effective duty cycle for the LBGs is small and most LBGs are associated with minor mergers or small-mass collisions. We note, however, that differences in the clustering properties and inferred host masses for the so-called "massive halo" model and the "collisional starburst" model may have been exaggerated — in the former case because the massive subhalos were ignored, and in the latter because the efficiency of star formation in mergers was probably overestimated (e.g., Cox et al. 2005).

A key success of the simulations and our model is the correct description of the small-scale upturn in the correlation function. At $z \sim 0$, the upturn is detected for bright galaxies (Zehavi et al. 2004), while the correlation function of faint objects is very close to a power law (Zehavi et al. 2005). At $z \gtrsim 1$, the upturn is more pronounced and is now unambiguously detected both in the DEEP2 data and in LBG samples at $z \sim 3-5$, as predicted from the halo model arguments (Zheng 2004)

and cosmological simulations (Kravtsov et al. 2004b). The trend towards more pronounced deviation from the power-law form of CF at higher z appears to be due to a couple different factors.

The accretion rate of subhalos is substantially higher at high z, so that the abundance of subhalos with masses close to the threshold mass of the sample, $M_{\rm min}$, is also larger on average (see § 5). This makes the "shoulder" of the HOD of high-z objects shorter and not as flat, increasing the number of small-separation pairs between central galaxies and satellites and between satellites themselves in *small-mass halos*. This also makes the width of the HOD at masses close to $M_{\rm min}$ wider and closer to the Poisson distribution. Although the overall fraction of subhalos in a given sample actually *decreases* with increasing redshift (see Fig. 1), the average mass of the distinct halos hosting most of subhalos is decreasing as well. The contribution of the pairs of objects within the same halo to the 1-halo term of the correlation function comes then predominantly from the smallest halos in the sample and the 1-halo term is considerably "peakier" than at lower redshifts, where halos of a wide range of masses contribute. We argue therefore that the more pronounced upturn in the correlation function at higher redshifts and for rarer objects at a given epoch is primarily due to the increased fraction of subhalos in host halos with masses closer to the threshold mass of the sample.

In the present work, we have not included any scatter in matching luminosity and velocity relations, and it is interesting that making this approximation works so well. Some scatter in the $L-V_{\rm max}$ relation should certainly be expected given the scatter in the observed Tully-Fisher and Faber-Jackson relations. This scatter likely depends on band, galaxy properties, and the extent to which internal dust extinction has been corrected for. For our purposes, the main effect of adding scatter in this relationship to our model would be at the highest luminosities. The insensitivity at low luminosities arises because 1) the luminosity function of galaxies is rather flat at $L < L_*$ so that the scatter results in almost equal numbers of objects scattering in and out of the sample, and 2) the bias of halos corresponding to these luminosity cuts ($L < L_*$), is only a weak function of mass and luminosity both in our simulations and in observations (Tegmark et al. 2004), so changes in the mass distribution of galaxies do not affect clustering significantly. In contrast, at higher luminosities, both the luminosity function and the bias dependence on mass are steep, and adding scatter serves to decrease the average clustering and makes the luminosity a steeper function of mass. Tasitsiomi et al. (2004) find that some scatter is required to match the galaxy-mass correlations, but the conclusion is reached using $V_{\rm max}^{\rm now}$ for subhalos, which we expect to exhibit more scatter with luminosity than $V_{\rm max}^{\rm acc}$. There is, however, an interesting tension between constraints provided by the observed galaxy-galaxy and galaxy-mass correlation functions for the most massive halos (cf. Fig. 3): the former constrains the scatter for bright galaxies to be small, while the latter appears to require significant amount of scatter. We postpone a full discussion of these issues including combined constraints to future work.

7. SUMMARY

Our main results and conclusions are as follows:

1. We show that a simple, non-parametric model which monotonically relates galaxy luminosities to the maximum circular velocity of dark matter halos, $V_{\rm max}$, by preserving the observed galaxy luminosity function, accurately reproduces the observed luminosity-dependent clustering of galaxies over projected separations $0.1 < r_p/(h^{-1}\ {\rm Mpc}) < 10.0$, through most of the evolution of the universe from $z \sim 5$ to the present.

2. The key to the success of the model is our luminosity assignment scheme, in which we use the maximum circular velocity at the time of accretion, $V_{\rm max}^{\rm acc}$, for subhalos and the maximum circular velocity at the time of observation, $V_{\rm max}^{\rm now}$, for distinct halos. We argue that for subhalos in dissipationless simulations, $V_{\rm max}^{\rm acc}$ reflects the luminosity and stellar mass of the associated galaxies better than the circular velocity at the epoch of observation, $V_{\rm max}^{\rm now}$

3. Our simulations, coupled with the above luminosity assignment scheme, correctly reproduce the small-scale deviation of the correlation function from the power-law form (the upturn) in observed luminosity-selected samples at different redshifts. The deviation is, in general, more pronounced at high redshifts. We attribute this trend to the increased fraction of satellite galaxies in host halos with masses close to the threshold mass of the sample.

4. Our luminosity assignment model applied to the simulations at $z \sim 3-5$ reproduces the observed shape and amplitude of the two-point correlation function of Lyman-break galaxies on both large and small scales. This suggests that LBGs are fair tracers of the overall halo population at these epochs and that their luminosity can be simply related to the circular velocity (and hence mass) of their dark matter halos. Although our model implies that most ($\sim 90\%$) of the LBGs are central galaxies in distinct halos, a fraction of the LBGs correspond to subhalos (i.e., satellites). This fraction is sufficiently high for a significant deviation of the LBG correlation function from the power law at small scales.

It is quite remarkable that, after vast improvements in observational data over the past decade, the simple picture for the formation of galaxies within virialized dark matter halos (White & Rees 1978; Fall & Efstathiou 1980), whereby galaxy properties such as luminosity are tightly coupled to the properties of their host halos, provides a good description of the observed clustering trends of galaxies over nearly the entire age of the Universe, on both large and small scales.

As we discussed above, our $L-V_{\rm max}$ model has natural implications for the Tully-Fisher relation and dynamical mass-to-light ratio, and the evolution in these quantities. A fruitful followup to the study presented here would be to compare the predictions of this model to local and to (forthcoming) DEEP2 measurements of

the relation. The comparison of model predictions to observed galaxy-galaxy and galaxy-mass clustering can also constrain the amount of scatter in the $L-V_{\rm max}$ relation for bright galaxies, and readily predicts the conditional luminosity function of galaxies (luminosity function as a function of distinct halo mass), and its evolution. Our luminosity assignment scheme can also be extended by separately modeling central and satellite galaxies, which appear to be two distinct populations with different origins and observable properties (Vale & Ostriker 2004; Cooray 2005a,b; Weinmann et al. 2005; Hansen et al. 2005).

The simulations were run on the Columbia machine at NASA Ames and on the Seaborg machine at NERSC (Project PI: Joel Primack). First and foremost, we would like to thank Anatoly Klypin for running these simulations and making them available to us. We are also indebted to Brandon Allgood for providing the merger trees that were used to measure $V_{\rm max}^{\rm acc}$. We thank Kurt Adelberger, Alison Coil, Mauro Giavalisco, Kyoungsoo Lee, and Masami Ouchi for providing access to and offering help with the interpretation of their data; and especially thank Alison Coil and the DEEP team for making their clustering data available to us in advance of publication. We additionally thank Andrew Zentner and Jeremy Tinker for useful discussions about the halo model and Oleg Gnedin for discussions about GOODS clustering analysis and useful comments on a draft of this manuscript. RHW is supported by NASA through Hubble Fellowship grant HST-HF-01168.01-A awarded by the Space Telescope Science Institute. AVK is supported by the National Science Foundation (NSF) under grants No. AST-0206216, AST-0239759 and AST-0507666, and by NASA through grant NAG5-13274. This research was carried out at the University of Chicago, Kavli Institute for Cosmological Physics and was supported in part by the grant NSF PHY-0114422. KICP is an NSF Physics Frontier Center. This work made extensive use of the NASA Astrophysics Data System and of the `astro-ph` preprint archive at `arXiv.org`.

REFERENCES

Abazajian, K., Zheng, Z., Zehavi, I., Weinberg, D. H., Frieman, J. A., Berlind, A. A., Blanton, M. R., Bahcall, N. A., Brinkmann, J., Schneider, D. P., & Tegmark, M. 2005, ApJ, 625, 613
Abazajian, K. et al. 2004, AJ, 128, 502
Adelberger, K. L., Steidel, C. C., Giavalisco, M., Dickinson, M., Pettini, M., & Kellogg, M. 1998, ApJ, 505, 18
Adelberger, K. L., Steidel, C. C., Pettini, M., Shapley, A. E., Reddy, N. A., & Erb, D. K. 2005, ApJ, 619, 697
Adelberger, K. L., Steidel, C. C., Shapley, A. E., Hunt, M. P., Erb, D. K., Reddy, N. A., & Pettini, M. 2004, ApJ, 607, 226
Adelberger, K. L., Steidel, C. C., Shapley, A. E., & Pettini, M. 2003, ApJ, 584, 45
Allgood, B. 2005, PhD thesis, University of California, Santa Cruz
Avila-Reese, V., Firmani, C., & Hernández, X. 1998, ApJ, 505, 37
Berlind, A. A., Weinberg, D. H., Benson, A. J., & et al. 2003, ApJ, 593, 1
Blanton, M. R. et al. 2003, ApJ, 592, 819
Blumenthal, G. R., Faber, S. M., Flores, R., & Primack, J. R. 1986, ApJ, 301, 27
Blumenthal, G. R., Faber, S. M., Primack, J. R., & Rees, M. J. 1984, Nature, 311, 517
Bower, R. G., Benson, A. J., Malbon, R., Helly, J. C., Frenk, C. S., Baugh, C. M., Cole, S., & Lacey, C. G. 2005, MNRAS submitted, arXiv:astro-ph/0511338
Brainerd, T. G. & Villumsen, J. V. 1992, ApJ, 400, 398
—. 1994a, ApJ, 431, 477
—. 1994b, ApJ, 425, 403
Bullock, J. S., Wechsler, R. H., & Somerville, R. S. 2002, MNRAS, 329, 246
Carlberg, R. G. 1991, ApJ, 367, 385
Coil, A. L. et al. 2004, ApJ, 609, 525
—. 2005a, ApJ, submitted, arXiv:astro–ph/0512233
—. 2005b, ApJ, submitted, arXiv:astro–ph/0507647
Cole, S., Aragon-Salamanca, A., Frenk, C. S., Navarro, J. F., & Zepf, S. E. 1994, MNRAS, 271, 781
Cole, S., Lacey, C. G., Baugh, C. M., & Frenk, C. S. 2000, MNRAS, 319, 168
Coles, P., Lucchin, F., Matarrese, S., & Moscardini, L. 1998, MNRAS, 300, 183
Colín, P., Carlberg, R. G., & Couchman, H. M. P. 1997, ApJ, 490, 1
Colín, P., Klypin, A. A., Kravtsov, A. V., & Khokhlov, A. M. 1999, ApJ, 523, 32
Cooray, A. 2005a, ApJ, submitted, arXiv:astro–ph/0509033
—. 2005b, ApJ, submitted, arXiv:astro–ph/0506087
Cooray, A. & Sheth, R. 2002, Phys. Rep., 372, 1
Cox, T. J., Jonsson, P., Primack, J. R., & Somerville, R. S. 2005, MNRAS submitted, arXiv:astro-ph/0503201
Croton, D. et al. 2005, ApJ, submitted, arXiv:astro–ph/0508046
Davis, M. et al. 2004, in "Observing Dark Energy", Sidney Wolff and Tod Lauer, editors, ASP Conference Series, arXiv:astro–ph/0408344
Diemand, J., Moore, B., & Stadel, J. 2004, MNRAS, 352, 535
Faber, S. M. et al. 2005, ApJ, submitted, arXiv:astro–ph/0506044
Fall, S. M. & Efstathiou, G. 1980, MNRAS, 193, 189
Gao, L., De Lucia, G., White, S. D. M., & Jenkins, A. 2004, MNRAS, 352, L1
Gerke, B. F. et al. 2005, ApJ, 625, 6
Giavalisco, M. & Dickinson, M. 2001, ApJ, 550, 177
Giavalisco, M., Steidel, C. C., Adelberger, K. L., Dickinson, M. E., Pettini, M., & Kellogg, M. 1998, ApJ, 503, 543
Hamana, T. et al. 2005, ApJ, submitted, arXiv:astro–ph/0508536
Hansen, S. M., McKay, T. A., Wechsler, R. H., Annis, J., Sheldon, E. S., & Kimball, A. 2005, ApJ, 633, 122
Hayashi, E., Navarro, J. F., Taylor, J. E., Stadel, J., & Quinn, T. 2003, ApJ, 584, 541
Jing, Y. P., Mo, H. J., & Boerner, G. 1998, ApJ, 494, 1
Jing, Y. P. & Suto, Y. 1998, ApJ, 494, L5
Katz, N., Hernquist, L., & Weinberg, D. H. 1999, ApJ, 523, 463
Kauffmann, G., Colberg, J. M., Diaferio, A., & White, S. D. M. 1999, MNRAS, 307, 529
Kauffmann, G., Guiderdoni, B., & White, S. D. M. 1994, MNRAS, 267, 981
Kazantzidis, S., Mayer, L., Mastropietro, C., Diemand, J., Stadel, J., & Moore, B. 2004, ApJ, 608, 663
Klypin, A., Gottlöber, S., Kravtsov, A. V., & Khokhlov, A. M. 1999, ApJ, 516, 530
Kolatt, T. S. et al. 1999, ApJ, 523, L109
Kravtsov, A. V. 1999, Ph.D. Thesis
Kravtsov, A. V., Gnedin, O. Y., & Klypin, A. A. 2004a, ApJ, 609, 482
Kravtsov, A. V. & Klypin, A. A. 1999, ApJ, 520, 437
Kravtsov, A. V., Klypin, A. A., & Khokhlov, A. M. 1997, ApJS, 111, 73
Kravtsov, A. V. et al. 2004b, ApJ, 609, 35
Lee, K.-S. et al. 2005, ApJ, submitted, arXiv:astro–ph/0508090
Lowenthal, J. D. et al. 1997, ApJ, 481, 673
Macció, A. V., Moore, B., Stadel, J., & Diemand, J. 2005, ArXiv Astrophysics e-prints
Mandelbaum, R., Seljak, U., Kauffmann, G., Hirata, C. M., & Brinkmann, J. 2005, MNRAS, submitted, arXiv:astro-ph/0511164
Mo, H. J., Mao, S., & White, S. D. M. 1998, MNRAS, 295, 319
—. 1999, MNRAS, 304, 175
Moore, B., Katz, N., & Lake, G. 1996, ApJ, 457, 455
Nagai, D. & Kravtsov, A. V. 2005, ApJ, 618, 557
Neyrinck, M. C., Hamilton, A. J. S., & Gnedin, N. Y. 2004, MNRAS, 348, 1
—. 2005, MNRAS, 362, 337

Norberg, P. et al. 2002, MNRAS, 332, 827
Ouchi, M. et al. 2004a, ApJ, 611, 660
—. 2004b, ApJ, 611, 685
—. 2005, ApJ, submitted, arXiv:astro–ph/0508083
Scannapieco, E. & Thacker, R. J. 2003, ApJ, 590, L69
Schechter, P. 1976, ApJ, 203, 297
Scoccimarro, R., Sheth, R. K., Hui, L., & Jain, B. 2001, ApJ, 546, 20
Seljak, U. 2000, MNRAS, 318, 203
Smith, R. E. et al. 2003, MNRAS, 341, 1311
Somerville, R. S. & Primack, J. R. 1999, MNRAS, 310, 1087
Somerville, R. S., Primack, J. R., & Faber, S. M. 2001, MNRAS, 320, 504
Steidel, C. & Hamilton, D. 1993, AJ, 105, 2017
Steidel, C. C., Adelberger, K. L., Dickinson, M., Giavalisco, M., Pettini, M., & Kellogg, M. 1998, ApJ, 492, 428
Steidel, C. C., Adelberger, K. L., Giavalisco, M., Dickinson, M., & Pettini, M. 1999, ApJ, 519, 1
Steidel, C. C., Adelberger, K. L., Shapley, A. E., Pettini, M., Dickinson, M., & Giavalisco, M. 2003, ApJ, 592, 728
Steidel, C. C., Giavalisco, M., Dickinson, M., & Adelberger, K. L. 1996, AJ, 112, 352
Tasitsiomi, A., Kravtsov, A. V., Wechsler, R. H., & Primack, J. R. 2004, ApJ, 614, 533
Tegmark, M. et al. 2004, ApJ, 606, 702
Tinker, J. L., Weinberg, D. H., Zheng, Z., & Zehavi, I. 2005, ApJ, 631, 41
Vale, A. & Ostriker, J. P. 2004, MNRAS, 353, 189
—. 2005, MNRAS submitted, arXiv:astro-ph/0511816
Wechsler, R. H., Gross, M. A. K., Primack, J. R., Blumenthal, G. R., & Dekel, A. 1998, ApJ, 506, 19
Wechsler, R. H., Somerville, R. S., Bullock, J. S., Kolatt, T. S., Primack, J. R., Blumenthal, G. R., & Dekel, A. 2001, ApJ, 554, 85
Weinmann, S. M., van den Bosch, F. C., Yang, X., & Mo, H. J. 2005, MNRAS, submitted, arXiv:astro-ph/0509147
White, S. D. M. & Frenk, C. S. 1991, ApJ, 379, 52
White, S. D. M. & Rees, M. J. 1978, MNRAS, 183, 341
Willmer, C. N. A. et al. 2005, ApJ, submitted, arXiv:astro–ph/0506041
Yan, R., Madgwick, D. S., & White, M. 2003, ApJ, 598, 848
Yang, X. et al. 2003, MNRAS, 339, 1057
York, D. G. et al. 2000, AJ, 120, 1579
Zehavi, I. et al. 2004, ApJ, 608, 16
—. 2005, ApJ, 630, 1
Zentner, A. R., Berlind, A. A., Bullock, J. S., Kravtsov, A. V., & Wechsler, R. H. 2005, ApJ, 624, 505
Zheng, Z. 2004, ApJ, 610, 61
Zheng, Z. et al. 2005, ApJ, submitted, arXiv:astro–ph/0408564